Biochimica et Biophysica Acta 1797 (2010) 304–313

Contents lists available at ScienceDirect

Biochimica et Biophysica Acta

journal homepage: www.elsevier.com/locate/bbabio

Inhibition of the [NiFe] hydrogenase from *Desulfovibrio vulgaris* Miyazaki F by carbon monoxide: An FTIR and EPR spectroscopic study

Maria-Eirini Pandelia, Hideaki Ogata, Leslie J. Currell, Marco Flores [1], Wolfgang Lubitz *

Max-Planck-Institut für Bioanorganische Chemie, Stiftstrasse 34-36, D 45470, Mülheim a.d. Ruhr, Germany

ARTICLE INFO

Article history:
Received 1 September 2009
Received in revised form 21 October 2009
Accepted 10 November 2009
Available online 17 November 2009

Keywords:
[NiFe] hydrogenase
Desulfovibrio vulgaris
Carbon monoxide inhibition
Spectro-electrochemistry
Rapid-scan FTIR
EPR

ABSTRACT

X-ray crystallographic studies [Ogata et al., *J. Am. Chem. Soc.* 124 (2002) 11628–11635] have shown that carbon monoxide binds to the nickel ion at the active site of the [NiFe] hydrogenase from *Desulfovibrio vulgaris* Miyazaki F and inhibits its catalytic function. In the present work spectroscopic aspects of the CO inhibition for this bacterial organism are reported for the first time and enable a direct comparison with the existing crystallographic data. The binding affinity of each specific redox state for CO is probed by FTIR spectro-electrochemistry. It is shown that only the physiological state Ni–SI_a reacts with CO. The CO-inhibited product state is EPR-silent (Ni^{2+}) and exists in two forms, Ni–SCO and Ni–SCO_{red}. At very negative potentials, the exogenous CO is electrochemically detached from the active site and the active Ni–R states are obtained. At temperatures below 100 K, photodissociation of the extrinsic CO from the Ni–SCO state results in Ni–SI_a that is identified to be the only light-induced state. In the dark, rebinding of CO takes place; the recombination rate constants are of biexponential character and the activation barrier is determined to be approximately 9 kJ mol^{-1}. In addition, formation of a paramagnetic CO-inhibited state (Ni–CO) was observed that results from the interaction of carbon monoxide with the Ni–L state. It is proposed that the nickel in Ni–CO is in a formal monovalent state (Ni^{1+}).

1. Introduction

Hydrogenases are metalloenzymes that catalyze the reversible conversion of molecular hydrogen according to: $H_2 \rightleftharpoons 2H^+ + 2e^-$ [1]. They are part of an energy converting mechanism found in the metabolic pathway of a wide variety of microorganisms [2]. They can be classified according to their metal content as: (a) [NiFe] hydrogenases with a hetero-binuclear Ni–Fe active center [3-5], (b) [FeFe] hydrogenases with a binuclear iron site connected to a [4Fe4S] cubane [6] forming the so-called H-cluster [7], and (c) iron–sulfur cluster-free hydrogenases (Hmd) consisting of a mononuclear iron site [8].

The [NiFe] hydrogenase from the sulfate reducing bacterium *Desulfovibrio vulgaris* Miyazaki F is a membrane attached enzyme with a molecular weight of 91.3 kDa [9], consisting of two subunits [10]. The large subunit (62.5 kDa) contains the Ni–Fe center [11]. This is shown in Fig. 1a. The two metals are connected via two cysteinyl residues and depending on the redox state of the enzyme, a third non-protein ligand is present at the active site (labeled X in Fig. 1a). The nickel ion is coordinated by two more cysteines (terminal) and changes during catalysis its redox state (Ni^{3+}, Ni^{2+} and maybe Ni^{1+}) [12]. The iron, in all intermediate states of the enzymatic cycle, maintains a low oxidation state (Fe^{2+}) and is coordinated by three diatomic inorganic ligands [13]; one carbonyl surrounded by hydrophobic residues and two cyanides that are hydrogen bonded to nearby amino acids [14]. The small subunit (28.8 kDa) harbors a $[3Fe4S]^{1+/0}$ center situated between two low potential $[4Fe4S]^{2+/1+}$ clusters [11,15,16]. These three clusters mediate the electron transfer between the [NiFe] center and the native electron acceptor cytochrome c_3 [1,17]. Proton transfer involves several possible pathways, among which the most predominant is via the glutamate residue (Glu34, *D. vulgaris* numbering) located near the nickel center [18].

In the presence of oxygen, reversible inhibition of the enzyme takes place. Purification is carried out aerobically and thus the protein is obtained in inactive states containing oxygen-based ligands in the bimetallic site. The two most oxidized forms are known as Ni–A and Ni–B [4,5] (Scheme 1). They are both paramagnetic (Ni^{3+}, $S=1/2$) [19], but differ in their spectroscopic and catalytic properties [20,21]. Ni–B is readily activated in the presence of H_2 or under reducing conditions, whereas Ni–A shows a long delay in its activation kinetics [21,22]. The difference in their activation rates has been recently ascribed to the different identities of the oxygenic ligands, OH^- for Ni–B [19,23], and a proposed OOH^- for Ni–A [23,24].

One-electron reduction of Ni–A and Ni–B leads to the Ni–SU and Ni–SI_r inactive states (Ni^{2+}, EPR-silent[2]) [25,26], respectively. For

* Corresponding author. Tel.: +49 208 306 3611; fax: +49 208 306 3955.
E-mail address: lubitz@mpi-muelheim.mpg.de (W. Lubitz).

[1] Present address: Department of Chemistry and Biochemistry, Arizona State University, Tempe, AZ 85287-1604, USA.

[2] Integer spin ground states can be characterized as EPR-silent either if they are diamagnetic ($S=0$) or if they cannot be observed by conventional microwave frequencies X/Q/W band frequencies (i.e., $S \geq 1$, where the zero field splitting is larger than the microwave quantum). So far no experimental evidence exists from high field EPR for the reduced hydrogenase states, whether they are associated with a high spin or low spin state for Ni^{2+}.

0005-2728/$ – see front matter © 2009 Elsevier B.V. All rights reserved.
doi:10.1016/j.bbabio.2009.11.002

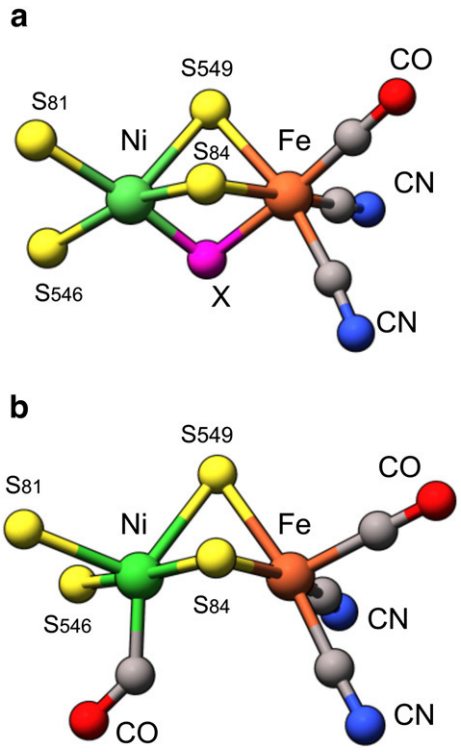

Fig. 1. (a) Representation of the active site of the [NiFe] hydrogenase from *D. vulgaris* Miyazaki F in the oxidized and H_2 reduced forms that carry an oxygenic or hydrogenic species, respectively. (b) The active site of the CO-inhibited hydrogenase (entry 1UBJ, protein databank). The elements are represented with the following colors: Fe (orange), Ni (green), S (yellow), C (grey), O (red), N (blue). The third bridging ligand X is shown in magenta.

Ni–SI_r, two states have been observed, $(Ni–SI_r)_I$ carrying an OH^- bridge and $(Ni–SI_r)_{II}$ with an H_2O bridge [27], which co-exist in acid–base equilibrium (Scheme 1). Catalytic activity is recovered in the Ni–SI_a state (Ni^{2+}, EPR-silent) by liberation of the oxygenic species. Further reduction leads to Ni–C, a paramagnetic state (Ni^{3+}, $S = 1/2$) with a hydride (H^-) bridging the two metals [28,29]. Ni–C is photosensitive at low temperatures, leading to the dissociation of the bridging H^- [28,30]. Further reaction of Ni–C with hydrogen produces Ni–R (Ni^{2+}, EPR-silent), which can exist in more than one protonation states [27,31].

It has been shown that carbon monoxide also inhibits the catalytic function of hydrogenase enzymes [32,33]. X-ray crystallographic experiments [34] have demonstrated that the exogenous CO ligand coordinates to the nickel (Fig. 1b). Two different CO-inhibited states have been observed, with distinct electronic structures and properties [32,36]. The formation of these states depends on the redox state and the coordination number of nickel. The paramagnetic form is known as Ni–CO [32,35], whereas the EPR-silent forms are known as Ni–SCO/Ni–SCO_{red} [36]. In all the above states, the exogenous CO ligand can be photodissociated from the active site at near cryogenic temperatures [32,34,35,37].

The present work presents an extensive spectroscopic characterization of the interaction between carbon monoxide and the [NiFe] hydrogenase from *D. vulgaris* Miyazaki F, for which, apart from a high resolution crystal structure [34], no previous information exists on the properties of the CO adduct(s). A thorough investigation consisting of infrared spectro-electrochemistry, rapid-scan FTIR and EPR is described and results are compared to those corresponding to hydrogenases from other organisms [35-38]. In particular, the activation barrier for the rebinding of CO to the active site of hydrogenases is determined and the paramagnetic Ni–CO state is described for the first time for a [NiFe] hydrogenase from sulfate reducing bacteria. Results are discussed within the framework of structural models proposed for the oxygen-sensitive hydrogenases.

2. Materials and methods

2.1. Purification of the enzyme

Hydrogenase from *D. vulgaris* Miyazaki F was purified from 50-l cultures as previously described [9]. The pH of the enzyme solutions was kept at pH 7.40 in Tris/HCl buffer for all experiments. In sample preparations, where the enzyme was incubated with carbon monoxide at 0 °C, with consideration of the temperature dependence of the Tris buffer, the pH for that case was calculated to be 8.12.

2.2. Reactions with gases

Reduction with H_2 (N 50, Air Liquide) and treatment with carbon monoxide gas (N 47, Air Liquide) and ^{13}CO labeled gas (<10% $^{18}O_2$, Cambridge Isotopes) were performed using a home-built gas mixer. Mixtures of gases (H_2, CO) were regulated with a manometer in a steel chamber of 30 cm^3.

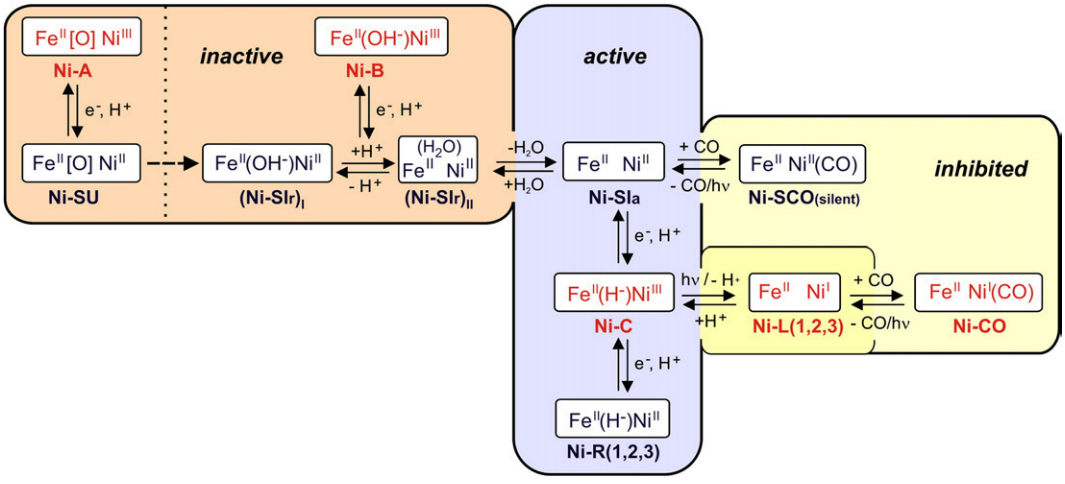

Scheme 1. Proposed mechanism for the [NiFe] hydrogenase from *D. vulgaris* Miyazaki F, including both active and inactive intermediate states. The orange-shaded frame contains the oxygen-inhibited inactive states, the light blue frame contains the active states, the light yellow contains the CO inhibited and the dark yellow frame contains the light-induced state(s). EPR-active states are indicated in red and EPR-silent states in blue.

2.3. Preparation of the Ni–SCO state

Two preparation procedures were used. The first consists of adding methyl viologen ($E_m = -448$ mV, Sigma Aldrich) as an electron acceptor to 50 μl of *D. vulgaris* hydrogenase. Final concentration of methyl viologen was 1.6 mM and that of the protein was 1 mM. Reduction for 3 min with H_2 (1.1 bar, ~22 °C) was followed by an incubation for 15 min with CO (2.5 bar, ~0 °C). Fifteen microliters were transferred into the FTIR sample cell and immediately frozen in liquid N_2. The remaining sample was used for control measurements (EPR spectroscopy). In the second procedure 50 μl hydrogenase (1 mM) were activated with H_2 (1.1 bar, ~22 °C) for 40 min and further incubated for 15 min with CO gas (2.5 bar, ~0 °C).

2.4. Preparation of the Ni–SCO_{red} state

The Ni–SCO state was prepared according to the second preparation procedure described above. The sample was further reduced by sodium dithionite (Sigma Aldrich) yielding mainly the Ni–SCO_{red} state.

2.5. Preparation of the paramagnetic Ni–CO state

Degassed hydrogenase samples were reduced for 30–50 min with hydrogen (1.1 bar, ~22 °C) and further incubated with either CO or CO/H_2 gas mixtures. Interaction solely with CO was restricted to 1 min; whereas interaction with gas mixtures of 20% CO/80% H_2 was carried out for 30 min. Samples were frozen in liquid N_2 under green light.

2.6. FTIR spectroscopy

Infrared measurements were carried out with a Bruker IFS 66v/S FTIR spectrometer equipped with a mercury–cadmium–telluride (MCT) photoconductive detector (Kolmar Technologies). For the experiments at 100 K and below, an Oxford Instruments OptistatCF cryostat with an ITC 503 temperature controller was used. The spectral resolution of the low temperature measurements was 2 cm^{-1}.

2.7. FTIR electrochemistry

Infrared electrochemical measurements were performed in an Optically Transparent Thin-Layer Electrochemical (OTTLE) cell described by Moss et al. [39,40], with 1 cm^{-1} spectral resolution. The mediators used for the titrations were: methyl viologen, benzyl viologen, neutral red, phenosafranine, anthraquinone-2-sulfonate, anthraquinone-1,5-disulfonate, 2-hydroxy-1,4-naphthoquinone, potassium indigo tetrasulfonate, methylene blue. The midpoint potentials of these mediators at pH 7.0 are given elsewhere [41]. Solubilization of the mediators was achieved by sonication on ice and addition of 5–10% glycerol. The protein solution for the electrochemical measurements contained 1 mM of hydrogenase, 125 μM of each mediator and 100 mM KCl (final concentrations). The enzyme-redox mediator solution was saturated for 15 min with carbon monoxide (2.5 bar, ~0 °C) and transferred to the electrochemical Moss cell under 100% CO atmosphere (glove bag). In the electrochemical cell [39], a layer of the protein-redox mediator solution is formed between two CaF_2 windows on an 8.5-μm-thick gold mesh in electrical contact with a platinum counter electrode. An Ag/AgCl electrode (1 M KCl) was used as a reference, which was calibrated prior to and after each measurement by the reduction of methyl viologen. In the titrations the potential was controlled with a potentiostat (Princeton Applied Research/EG&G Model 283) and the temperature was maintained with a thermostat (RML6 LAUDA) at the desired value. After full activation of the enzyme a time period of 3–5 min was required to reach redox equilibrium at each applied potential. All potentials in this work are quoted versus the normal hydrogen electrode (NHE). Data were collected and baseline corrected using the OPUS software (Bruker). Data fitting was performed using MATLAB 7.0. The measured areas of the bands were normalized by dividing with the enzyme concentration and the optical path length. In this way the apparent integrated absorption intensity (B, mM^{-1} cm^{-1}) was obtained.

2.8. Rapid-scan FTIR

Fifteen-microliter hydrogenase samples were placed between sapphire windows (80-μm path length) and inserted in the cryostat at low temperatures. The samples were illuminated *in situ* for 5 min (halogen lamp 24 V, 250 W) prior to measuring the recombination kinetics in the rapid-scan mode. The time resolution of the rapid-scan measurements was in the order of 1 s. The temperature dependence of the measured kinetic rates was fitted with the Arrhenius equation ($\ln k = \ln A_0 - E_a/RT$) [42], where k is the rate constant (s^{-1}), A_0 is the frequency factor (s^{-1}), E_a is the activation energy (kJ mol^{-1}), R is the ideal gas constant (8.314 J K^{-1} mol^{-1}) and T is the temperature in K.

2.9. EPR spectroscopy

EPR measurements were carried out with a Bruker E-300 c.w. X-band spectrometer using a rectangular cavity (TE_{102}) and an Oxford Instruments helium flow cryostat with an ITC 503 temperature controller. Illumination of the samples at low temperatures was performed in the EPR resonator with a halogen lamp (12 V, 50 W) until maximum conversion was obtained (~5 min).

3. Results

3.1. FTIR electrochemistry at room temperature (inactivated enzyme)

The redox chemistry of the [NiFe] hydrogenase from *D. vulgaris* was investigated by infrared electrochemical studies in enzyme solutions with and without carbon monoxide. FTIR probes changes in the active site (e.g., electron density at the Fe, coordination number, hydrogen bonding) [43,44], by means of monitoring the stretching vibrations of the CO and CN^- ligands. Each redox state is thus characterized by three IR bands [13], one for a terminally bound carbonyl in the region 1900 to 1970 cm^{-1}, and two corresponding to the coupled vibrations of the two cyanide ligands in the region 2100 to 2040 cm^{-1}. The infrared absorption bands of all redox intermediates at room temperature are collected in Table 1. In the text, the

Table 1
Stretching vibrations of the CO and CN^- ligands for each redox state of the [NiFe] hydrogenase from *D. vulgaris* Miyazaki F at 25 °C (298 K).

State	IR frequencies (cm^{-1})			
	$\tilde{\nu}_{CO}(Fe)$	$\tilde{\nu}^{asym}{}_{CN}(Fe)$	$\tilde{\nu}^{sym}{}_{CN}(Fe)$	$\tilde{\nu}_{CO}(Ni)$
Ni–A	1956	2085	2094	–
Ni–B	1955	2081	2090	–
Ni–SU	1958	2089	2100	–
$(Ni–SI_r)_I$	1921	2061	2070	–
$(Ni–SI_r)_{II}$	1943	2074	2086	–
$Ni–SI_a$	1943	2074	2086	–
	(1946)	(2077)	(2090)	(–)
Ni–C	1961	2074	2085	–
Ni–R(1)	1948	2061	2074	–
Ni–R(2)	1932	2052	2066	–
Ni–SCO	1941	2071	2084	2056
	(1941)	(2072)	(2086)	(2061)
$Ni–SCO_{red}$	1939	2070	2083	2054
	(1940)	(2071)	(2086)	(2060)

Values at 100 K are given in parenthesis.

characteristic stretching vibration of the CO band for each state is given in parenthesis.

Fig. 2a shows the FTIR spectrum of the aerobically isolated hydrogenase from *D. vulgaris* at +229 mV (25 °C). In this spectrum the bands corresponding to the oxygen inhibited forms Ni–A, Ni–B and $(Ni–SI_r)_I$ could be identified [26] (Scheme 1, Table 1). The Ni–B and Ni–A states were shown by EPR experiments to occur in a ratio 7:3. The CO band in Fig. 2a results from the overlap of Ni–B (1955 cm^{-1}) and Ni–A (1956 cm^{-1}) and is thus centered at 1955 cm^{-1}. The Ni–SU state could not be resolved in these spectra (Table 1). A CO band of small intensity at 1964 cm^{-1} was observed, but the corresponding CN^- bands could not be identified. This state, denoted as $Ni–S_{1964}$, is EPR-silent. It can be electrochemically reduced irreversibly and its yield does not depend on pH. The FTIR spectrum in the case of the aerobically purified hydrogenase in a carbon monoxide saturated buffer solution under 100% CO atmosphere was identical (Fig. S1 of the Supplementary data).

Fig. 2b shows the spectrum of hydrogenase partially activated for 53 min at −295 mV in the absence of CO. Reduction of Ni–B (1955 cm^{-1}) resulted in the increase of the $(Ni–SI_r)_I$ (1921 cm^{-1}) state and the appearance of $(Ni–SI_r)_{II}$ and/or $Ni–SI_a$ (1943 cm^{-1})[3]. Fig. 2c shows the spectrum of the CO saturated hydrogenase after 53 min at −95 mV. A second sample of CO saturated hydrogenase poised for 30 min at −295 mV is shown in Fig. 2d. In both spectra the dominant species is the CO-inhibited state Ni–SCO (1941 cm^{-1}), as confirmed by the appearance of an additional fourth band at 2056 cm^{-1}, originating from the binding of exogenous CO to nickel [34,37,38]. Activation of the [NiFe] hydrogenase in the presence of carbon monoxide proceeds faster and at more positive redox potentials.

3.2. FTIR electrochemistry at room temperature (fully activated enzyme)

Fig. 3 collects the infrared spectra of the fully activated [NiFe] hydrogenase from *D. vulgaris* without CO (left) and with CO (right) in solution, poised at different redox potentials. At a potential of −228 mV (Fig. 3a, left), the hydrogenase is predominantly at the onset of its catalytic cycle with its major fraction in the $Ni–SI_a$ state (1943 cm^{-1}). A small band corresponding to the $(Ni–SI_r)_I$ (1921 cm^{-1}) is also present. In the carbon monoxide saturated protein at the same potential (Fig. 3a, right), all of the enzyme molecules are in the EPR-silent Ni–SCO state (1941 cm^{-1}).

At a potential of −419 mV (Fig. 3b, left), the main state observed in the activated enzyme is Ni–C (1961 cm^{-1}). A second state with its CO band centered at 1948 cm^{-1} corresponds to Ni–R(1). At the same redox potential in the CO saturated protein (Fig. 3b, right), the hydrogenase remains in the Ni–SCO state. However, the bands are now shifted by approximately 0 to 1 cm^{-1} to lower wave numbers. At a potential of −499 mV (Fig. 3c, left), the most reduced Ni–R(1) state (1948 cm^{-1}) increases in intensity relative to Ni–C (1961 cm^{-1}). At the same redox potential (Fig. 3c, right) in the CO saturated enzyme, the bands corresponding to Ni–SCO shift again toward lower frequencies. The intrinsic CO band is now centered at 1939 cm^{-1} and the band of the exogenous CO is at 2054 cm^{-1}. The bands corresponding to the coupled cyanides are also shifted by 1 cm^{-1} with respect to the spectrum at −228 mV (Fig. 3a, right). This small but consistent shift has been associated previously with a state denoted as $Ni–SCO_{red}$ in the hydrogenase from *Desulfovibrio fructosovorans* [36]. This effect is fully reversible upon electrochemical reoxidation. EPR experiments showed that the $Ni–SCO_{red}$ state is EPR-silent (data not shown, see Discussion). In addition, in this spectrum a small fraction of Ni–C (1961 cm^{-1}) is also observed (Fig. 3c, right).

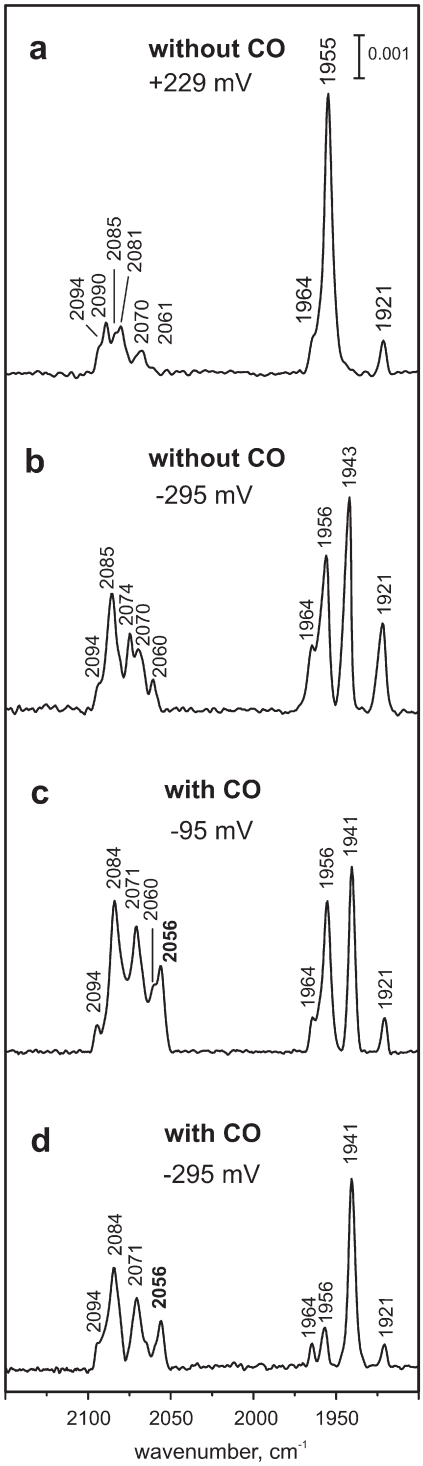

Fig. 2. FTIR spectra of the *D. vulgaris* Miyazaki F [NiFe] hydrogenase in the absence of CO in the solution (a) at +229 mV and (b) partially activated for 53 min at −295 mV. In the presence of CO in solution (c) partially activated sample for 53 min at −95 mV and (d) a second sample partially activated for 30 min at −295mV. All redox potentials are quoted vs. NHE and the temperature is 25 °C. The *y*-axis in all figures represents the IR absorbance.

At a potential of −639 mV in the absence of CO (Fig. 3d, left), most of the sample is in the Ni–R(1) state (1948 cm^{-1}, ~53%), while smaller fractions are in Ni–C (1961 cm^{-1}, ~23%) and Ni–R(2) (1932 cm^{-1}, ~ 24%). Lowering the potential to −739 mV (Fig. 3e, left) results in an increase of the intensity of Ni–R(2) relative to Ni–C and Ni–R(1). In the CO saturated

[3] The $(Ni–SI_r)_{II}$ inactive state has a water molecule as ligand weakly bound at its active site. The active $Ni–SI_a$ state has no additional X ligand (see Fig. 1) and the divalent nickel is four-coordinated. However, both states are described by the same FTIR spectrum [26], indicating a very similar electronic distribution in the [NiFe] center of these states.

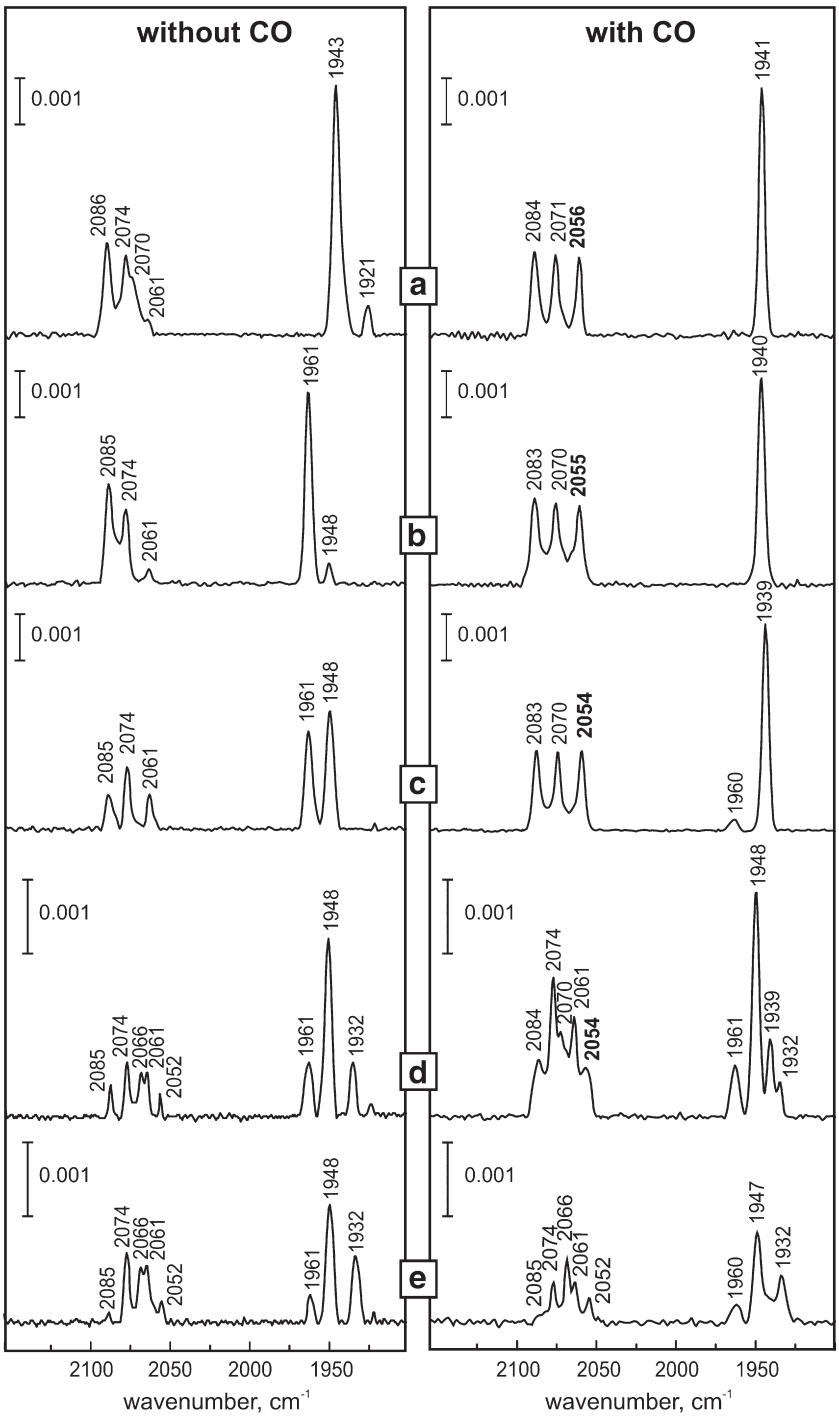

Fig. 3. FTIR spectra of the *D. vulgaris* Miyazaki F [NiFe] hydrogenase poised at different potentials. In the absence of CO in solution (left): (a) at −228 mV the Ni–SI_a is the major species, (b) at −419 mV the Ni–C is maximized, (c) at −499 mV a mixture of the Ni–C/Ni–R(1) states co-exist, (d) at −639 mV the Ni–R(1) state has maximal intensity and the Ni–R(2) appears, whose intensity increases (e) at −739 mV. For the CO saturated hydrogenase (right): (a) at −228 mV all the enzyme is in the Ni–SCO state, (b) at −419 mV and (c) at −499 mV the Ni–SCO_{red} is observed. At even lower potentials (d) at −639 mV and (e) at −739 mV the hydrogenase appears to have recovered from CO inhibition.

enzyme at −639 mV, Ni–R(1) becomes the species with the largest intensity and only a small fraction of the sample remains in Ni–SCO_{red} (Fig. 3d, right). At the more negative potential of −739 mV (Fig. 3e, right), Ni–SCO_{red} has completely disappeared and the sample contains a mixture of the catalytically active states (Ni–C, Ni–R(1), Ni–R(2)).

Assuming that Ni–SCO (1941 cm^{-1}) and Ni–SCO_{red} (1939 cm^{-1}) are two different forms of the same redox state, their apparent integrated intensity was plotted against the applied potential (Fig. 4). The data obtained from deconvolution of the two bands are best fitted with Nernstian curves corresponding to a one-electron transfer. The apparent midpoint potential of such a process at 25 °C was determined by the mean value of the two curves to be −421 mV ± 5 mV. In the same figure the potentiometric titration corresponding to the transition from Ni–SCO_{red} to Ni–R(1) is also shown. The apparent midpoint potential of this process was determined to be −596 mV ± 5 mV.

Reoxidation of the sample containing the active states (Ni–C, Ni–R (1,2)) in the presence of CO at 25 °C in the electrochemical cell yielded the Ni–SCO state. Binding of CO was faster than the insertion of oxygen in the active site. However, reoxidation of the sample from the

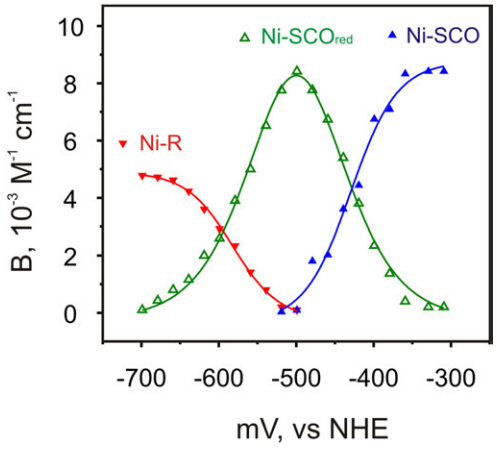

Fig. 4. Potentiometric titration at 25 °C for the Ni–SCO/Ni–SCO_{red} and Ni–SCO_{red}/Ni–R(1) pairs. The integrated absorption bands corresponding to Ni–SCO and Ni–SCO_{red} are plotted against the potential, corresponding to a one-electron transfer with apparent midpoint potential of −421 mV ± 5 mV. The data obtained from integration of the absorption bands corresponding to Ni–SCO_{red} and Ni–R(1) in the range between −499 mV and −719 mV are described by curves with an apparent midpoint potential of −596 mV ± 5 mV. The titration was fully reversible at 25 °C.

active states in the presence of CO at 4 °C resulted in the formation of Ni–B in approximately one third of the hydrogenase molecules in the sample (Fig. S2 of the Supplementary data).

3.3. FTIR experiments at low temperatures: Photodissociation of CO from the Ni–SCO state

Fig. 5a shows the FTIR spectrum of the Ni–SCO state at 40 K. The shifts observed in the positions of the bands with respect to those measured at room temperature (Fig. 3a, right) result from the more restricted vibrational motion of the diatomic molecules [45]. Four bands can be clearly observed in the spectra. The absorption band at 1941 cm^{-1} corresponds to the CO terminally bound to iron and the two peaks at 2072 and 2086 cm^{-1} are assigned to the conjugate CN^- ligands. A fourth additional band at 2061 cm^{-1} corresponds to the externally added CO bound to nickel. A similar spectrum has been obtained for the Ni–SCO state of the [NiFe] hydrogenase from *Allochromatium vinosum* [37,38], in which an absorption band at 2060 cm^{-1} was ascribed to the extrinsic CO. Inhibition of hydrogenase using isotopically labeled ^{13}CO results in the spectrum shown in Fig. 5b. The absorption band corresponding to the externally added CO shifts by 46 cm^{-1} to 2015 cm^{-1}, whereas the positions corresponding to the intrinsic ligands bound to iron remain unchanged.

It is known that the external CO can be photodissociated from the active site at temperatures below 100 K [32,34,37]. The spectrum after illumination at 40 K is shown in Fig. 5c. In this spectrum only three bands are observed, which correspond to the CO and the CN^- ligands bound to Fe. The fourth band associated with the external CO at 2061 cm^{-1} (or at 2015 cm^{-1}, in Ni–$S^{13}CO$) is absent, showing that the external CO is no longer attached to the active site. The light-induced state corresponds to the Ni–SI_a state (Table 1). Dissociation of the exogenous CO ligand occurs at temperatures equal to or lower than 100 K, but a complete photoconversion to Ni–SI_a (100% of the molecules in Ni–SCO) takes place only below 50 K.

3.4. Rapid-scan FTIR: Kinetics and activation energy for the reassociation of CO in the Ni–SI_a state

In the absence of light, the dissociated carbonyl ligand rebinds to the active site and the Ni–SCO state is reformed. This process is

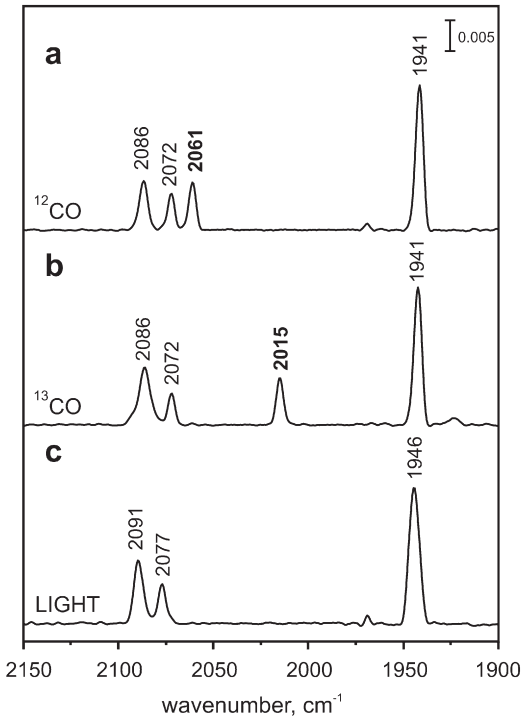

Fig. 5. (a) FTIR spectrum of the CO-inhibited enzyme from *D. vulgaris* Miyazaki F at 40 K in the dark. The absorption band of the exogenous CO is found at 2061 cm^{-1}. (b) ^{13}CO-inhibited hydrogenase in the dark at 40 K. The band of the exogenous ^{13}CO shifts by 46 cm^{-1} toward lower frequencies with respect to the exogenous ^{12}CO band. (c) After illumination, the absorption bands at 2061 cm^{-1} (and 2015 cm^{-1}, respectively) disappear, corresponding to the light dissociation of the externally added CO molecule. The light excited state is the Ni–SI_a state (1946 cm^{-1}).

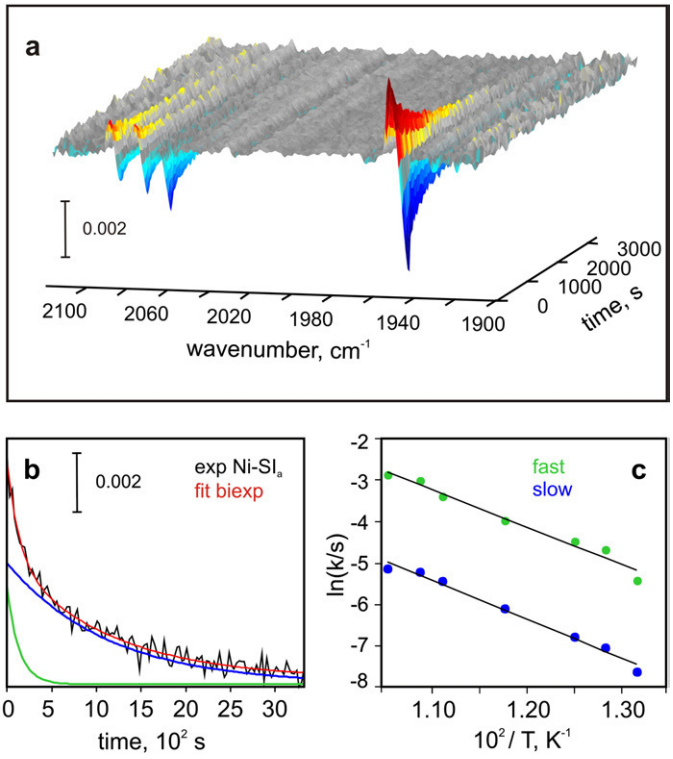

Fig. 6. (a) Three-dimensional representation of an FTIR light-minus-dark difference spectrum corresponding to the back conversion from Ni–SI_a to Ni–SCO as a function of the dark adaptation time at 78 K. (b) Time-dependent kinetics of the disappearance of the Ni–SI_a state in the dark was exponential and fitted by a biexponential model. The respective slow and fast components are shown in green and light blue. (c) Arrhenius plot for the fast and slow rebinding processes between 78 K and 95 K.

Table 2
Activation energies (E_a) for the rebinding of exogenous CO.

State	Type of fitting	E_a (kJ mol^{-1})
Ni–SCO/Ni–SI$_a$	Biexponential (fast)	8.0
	Biexponential (slow)	8.8
	Single exponential	9.2

The error in the determination of energies is ±8%.

completely reversible. Fig. 6a shows the time dependence of a light-minus-dark difference infrared spectrum in a three-dimensional representation at 78 K. The positive bands correspond to the Ni–SI$_a$ state (light product) and the negative bands correspond to Ni–SCO (educt state). At time $t=0$, the first slice of the spectrum represents the maximum difference, i.e., the maximum conversion from Ni–SCO to Ni–SI$_a$. As the time of dark adaptation is incremented, Ni–SCO recovers and Ni–SI$_a$ decreases in intensity. The resulting kinetics are biexponential, consisting of fast and slow components.

In Fig. 6b the kinetics of the disappearance of the Ni–SI$_a$ state are shown along with the corresponding data fits and components. No other intermediate states were detected within the time resolution of these experiments. The temperature dependence of the rate constants was examined in the range between 78 and 95 K for both slow and fast reassociation processes (Fig. 6c). The activation barrier for the reassociation of the extrinsic CO ligand was estimated by analyzing the kinetics of both the Ni–SCO recovery and the Ni–SI$_a$ disappearance, which were the same (within experimental error). The activation energy corresponds to approximately 9 kJ mol^{-1}. Results are summarized in Table 2. Activation energies assuming single exponential back conversion kinetics are also included.

3.5. EPR experiments: Formation of the paramagnetic Ni–CO state

In the present study, the interaction of CO with the [NiFe] hydrogenase from *D. vulgaris* Miyazaki F under physiological conditions yielded only one state in two different EPR-silent forms (Ni–SCO and Ni–SCO$_{red}$). Ni–SCO was shown to be light sensitive, which was also found for the catalytically active Ni–C state. However, reassociation of CO to the active site takes place at lower temperatures as compared to the rebinding of the hydrogenic species in the Ni–C state [30]. On the basis of this observation, the hydrogen reduced hydrogenase (Ni–C) was allowed to interact for only 1 min with carbon monoxide (see Experimental procedures). The respective EPR spectrum at 40 K (Fig. 7a) shows no changes in the Ni–C state signal ($g_x=2.20$, $g_y=2.15$, $g_z=2.01$) [29], except for a decrease of approximately 20% in its signal intensity (data of Ni–C without CO in the frozen solution are not shown). Illumination of the sample for 5 min at 40 K in the resonator of the EPR spectrometer resulted in the formation of the Ni–L state, described by a signal with values $g_x=2.30$, $g_y=2.12$, and $g_z=2.05$ (Fig. 7b). An additional rhombic signal was also present in both spectra ($g_x=2.21$, $g_y=2.09$ and $g_z=2.03$). This corresponds to a non-light-sensitive state and its amount depends on the purification procedure; it has previously been observed when the enzyme was treated with CO or Na_2S [24,58]. Based on the *g*-values and its relaxation behavior, it is most likely associated with a different conformation of the [NiFe] active site. To create the paramagnetic Ni–CO state, CO has to compete with the hydron for binding to the site of the Ni–L state [35]. Dark adaptation of Ni–L at 77 K showed, along with the Ni–C state, a new signal with a rhombic *g*-tensor. This signal is similar to the one observed in *A. vinosum* [32,35] and in *Methanococcus voltae* [46] hydrogenases treated with CO and is associated with a paramagnetic Ni–CO state. Dark adaptation after a second illumination of the sample yielded the maximum amount of EPR-detectable Ni–CO in the spectrum (Fig. 7c), in which all *g*-values can be clearly identified ($g_x=2.13$, $g_y=2.08$ and $g_z=2.02$).

4. Discussion

4.1. Electrochemical titrations and redox equilibria

Carbon monoxide has a high affinity for binding to transition metals [47]. In the case of the [NiFe] hydrogenases, binding of CO to the active site [34] is a process that hinders catalytic function and renders the enzyme inactive [33]. In the present work, a series of electrochemical measurements was carried out for the [NiFe] hydrogenase from *D. vulgaris* Miyazaki F and redox changes were followed by FTIR. The results can be summarized as follows:

(1) Carbon monoxide interacts only with the catalytically active state Ni–SI$_a$, in line with previous observations [48,49]. The FTIR spectrum of Ni–SCO strongly resembles that of Ni–SI$_a$ with respect to the bands of the diatomic Fe ligands, which show a constant shift of 2 to 3 cm^{-1}. This suggests that the active site conformation is only slightly distorted after binding extrinsic CO to nickel. The stretching vibration of the external CO centered at 2056 cm^{-1} suggests a weak π back-bonding, further supported by the X-ray structures of the CO adduct in *D. vulgaris*, which showed a terminally bound CO ligand with a bond length of 1.136 Å [34], close to the one for a free CO molecule (1.13 Å).

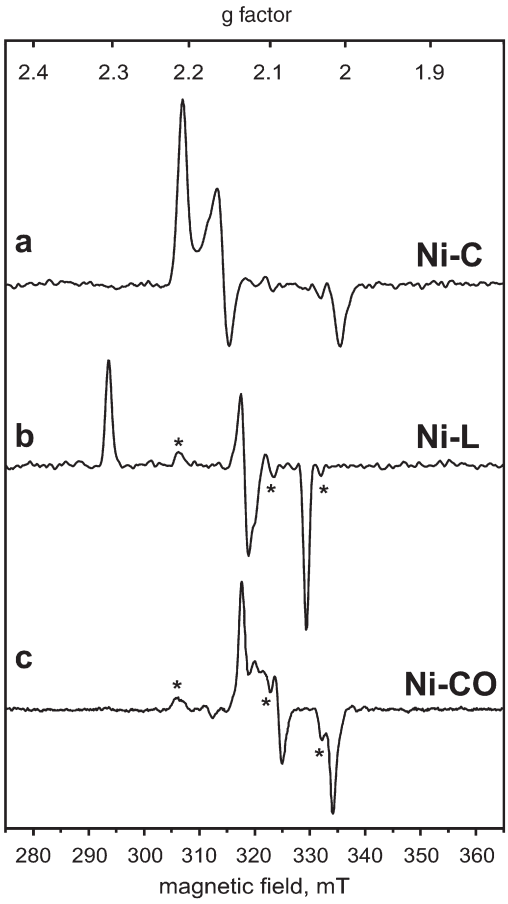

Fig. 7. EPR spectra of the [NiFe] hydrogenase from *D. vulgaris* Miyazaki F at 40 K. (a) Enzyme of the H_2 reduced sample (Ni–C) after interaction for 1 min with carbon monoxide, (b) same as (a) but after illumination for 5 min (Ni–L state). A rhombic non-light-sensitive signal often observed is denoted with an asterisk (see text). (c) The same sample after a second illumination–dark adaptation cycle (dark adaptation was carried out at 77 K). The majority of the enzyme is in the Ni–CO state described by a rhombic *g*-tensor with principal values $g_x=2.13$, $g_y=2.080$ and $g_z=2.019$. Experimental conditions: $T=40$ K, microwave frequency 9.454 GHz, modulation amplitude 0.7 mT, microwave power 2 mW, except for (c), which was 6 mW.

CO does not bind to the oxygen inhibited states (e.g., Ni–A, Ni–B, $(Ni–SI_r)_I$,) or to the active Ni–C/Ni–R states due to the presence of more electronegative ligands in the active site of these states and the overall electronic properties of the [NiFe] complex, which has a distorted octahedral geometry. In Ni–SI_a however, the nickel ion is in the divalent state and most of the proposed catalytic schemes are consistent with a four-coordinated nickel in a high spin state ($S=1$), which would retain the octahedral geometry of the complex [5,50]. A recent theoretical study showed that only models of Ni–SCO, considering a high spin nickel state, could reproduce the FTIR experimental results [51]. Therefore, the absence of additional non-protein ligands in the active site (i.e., oxo-based species or substrate-related ligands) and the electronic configuration of the nickel ion govern the interaction of CO with the [NiFe] center resulting in binding of carbon monoxide only to the active Ni–SI state.

(2) Hydrogenase is shown to be reactivated from the oxygen inhibited forms easier in the presence of CO. It was observed that in the presence of CO, transition to the functional intermediates occurs at significantly higher redox potentials than without CO (Fig. 2). This finding has been reported in various studies [52,53] but so far no definite explanation for this acceleration in the activation times has been substantiated.

(3) At an applied potential of −419 mV, a small shift in the bands of Ni–SCO (1 to 2 cm^{-1} toward lower frequencies) was observed, which was maximized at −499 mV (Ni–SCO_{red}). All four vibrational bands shifted slightly, suggesting a redistribution of the delocalized electronic density at the [NiFe] site [54]. To correlate formation of Ni–SCO_{red} (1939 cm^{-1}) with a possible redox change of nickel, the Ni–SCO state was reduced with sodium dithionite and the EPR spectrum was recorded. No additional signals could be observed, except for a weak Ni–C signal (data not shown). Both Ni–SCO and Ni–SCO_{red} are thus EPR-silent, as previously demonstrated [36]. Conversion from Ni–SCO to Ni–SCO_{red} was reversible and could be titrated as a one-electron process. Such a transition involves no redox change in the binuclear active site but is suggested to be connected with reduction of the proximal $[4Fe4S]^{2+/1+}$ cluster. This has been shown previously for the [NiFe] hydrogenase from *D. fructosovorans*, by comparing the UV/VIS spectra of the Ni–SCO/Ni–SCO_{red} states [36]. The midpoint potential found here is in good agreement with the redox potential for the reduction of the $[4Fe4S]^{2+/1+}$ proximal cluster in *D. vulgaris* [55]. A change in the electrostatic interaction between the proximal $[4Fe4S]^{2+/1+}$ cluster and the [NiFe] site therefore alters the electron density distribution on the bimetallic site, resulting in the small shift of the infrared bands.

(4) At −499 mV, the Ni–C state is present in the spectrum of Ni–SCO_{red} (Fig. 3c, right), whereas at more negative potentials a small increase of Ni–C and a larger increase of the Ni–R states is observed (Fig. 3d and f, right). A form of electrochemical cleavage of the Ni-CO bond of the externally added CO appears to take place, which is complete at −739 mV. At this potential only the active states (i.e., Ni–C, Ni–R(1,2)) were detected (Fig. 3e, right). Transition from Ni–SCO_{red} to Ni–R(1) was fitted as a one-electron process with a midpoint potential of −596 mV (Fig. 4). The appearance first of the Ni–C state and the involvement of one electron from the Ni–SCO_{red} to the Ni–R transition leads to the conclusion that upon removal of the external CO ligand, hydrogenase is left in the Ni–SI_a state. Depending on the potential and on the amount of redox equivalents, transition to Ni–R from the Ni–SI_a state takes place with or without Ni–C as a detectable intermediate. This has been shown by stopped-flow infrared studies on *A. vinosum* [38,49], where in the presence of excess hydrogen and with both [4Fe4S] clusters reduced, a direct transition of Ni–SI_a to Ni–R was observed. Most likely, in this case, Ni–C is an extremely short-lived intermediate. In addition, appearance of the Ni–C state under very reducing conditions (below the redox potential for the H_2/H^+ couple) results from the [NiFe] hydrogenase turnover (H_2 evolution) activity.

4.2. ^{13}CO isotope labeling

Isotopic labeling of Ni–SCO with ^{13}CO shifts the band of the extrinsic carbonyl by 46 cm^{-1} toward lower wave numbers (larger reduced mass relative to ^{12}CO). This shift is in agreement with that theoretically predicted for a "pure" CO vibration ($\tilde{\nu}_{13CO}=0.97771\cdot\tilde{\nu}_{12CO}$) [56]. In this case, the Cotton Kraihanzel Force Field (CKFF) [57,58] approximation permits calculation of the stretching parameters, by taking into account only the CO displacement and ignoring the metal carbonyl frequencies. An estimation of the force constants and the extent of metal-to-carbon π donation can be made. A relatively small force constant[4] $k\sim 1665$ N/m was obtained, showing a weak π back-bonding with a small degree of metal-to-carbon electron donation. The FTIR bands corresponding to the intrinsic carbonyl and cyanide ligands bound to iron do not shift upon labeling. This shows that there is no vibrational coupling between these diatomic oscillators and the externally added CO bound to nickel.

4.3. Photodissociation and reassociation kinetics of the external CO ligand to nickel

In Ni–SCO, the extrinsic CO is photolabile at temperatures ≤100 K. The light-induced state corresponds to Ni–SI_a. The infrared bands of the Fe ligands associated with Ni–SI_a, occur at higher frequencies compared to those of Ni–SCO. This indicates that dissociation of the carbonyl ligand (2061 cm^{-1}) at the nickel results in a small decrease of the electron density at the iron. Illumination of Ni–SCO_{red} (data not shown) also resulted in the formation of Ni–SI_a but was only effective at temperatures below 80 K. These results show that Ni–SI_a and not Ni–R(1,2) binds CO, leading to formation of the EPR-silent Ni–SCO/Ni–SCO_{red} states.

The cleavage of the Ni–CO bond upon illumination is reversible at $T\leq 100$K. Rebinding of CO takes place in the dark following biexponential kinetics, consisting of slow and fast components (Table 2). Such a biphasic nature could have a physical interpretation, since the CO ligand does not bind in a linear form to nickel, but the bonding is governed by an angle distribution $161°\leq\varphi\leq 136°$ [34]. This spread in the bonding modes could account for the composite nature of the recombination kinetics observed. Due to the restricted mobility of the bound carbonyl at these temperatures, the slightly different conformations are almost degenerate. This is illustrated in the activation energies for the rebinding of CO, which are very similar (Table 2). The activation barrier was estimated to between 8 and 9 $kJ\cdot mol^{-1}$. Transition from Ni–SI_a to Ni–SCO is a first-order process without intermediates. The back conversion kinetics for the disappearance of Ni–SI_a and increase of Ni–SCO are exponential, in contrast to the rebinding of CO to myoglobin (Mb) [60,61] in a similar temperature range. Activation energies for CO rebinding in Mb are between 5 and 30 kJ mol^{-1} [60–62], which are comparable to or even larger than the energy threshold required for the carbonyl to rebind to nickel in hydrogenases. These results show a considerable degree of similarity in the rebinding of CO to divalent transition metals (i.e., Ni^{2+}, Fe^{2+}), which may be of significance as both proteins are reversibly inhibited by CO.

[4] The force constant k for a free CO molecule considering an infrared frequency $\tilde{\nu}=2153$ cm^{-1} is 1872 N m^{-1}.

4.4. The paramagnetic Ni–CO state

In the present work, the paramagnetic Ni–C state was shown not to interact with CO, in agreement with previous studies [35]. Incubation with carbon monoxide results in the gradual disappearance of the EPR signal corresponding to Ni–C (Fig. 7a). This occurs as the concentration of CO in the protein solution becomes high enough to shift the redox equilibrium toward the Ni–SI_a state (Ni^{2+}, EPR silent), in which CO can bind.

Ni–C is light sensitive and illumination leads to the paramagnetic Ni–L state. The bridging hydride has been proposed to be dissociated as a proton, which would leave the nickel in a formally monovalent state (Ni^{1+}) [2,35,63] in Ni–L[5]. Dark adaptation of Ni–L in the presence of CO leads to the paramagnetic Ni–CO state (Fig. 7c), as rebinding of CO to the active site occurs at lower temperature with respect to the recombination of the hydrogenic species [30]. The paramagnetic Ni–CO has been well studied in *A. vinosum* [32,35] and *M. voltae* [46], whereas the present study is the first report for a hydrogenase from sulfate reducing species such as *D. vulgaris* Miyazaki F. Ni–CO is described by a rhombic spectrum with *g*-values significantly smaller than those of the other paramagnetic states of hydrogenase (i.e., Ni–A, Ni–B, Ni–C) [4]. This is a consequence of the binding of CO to nickel, which results in a larger ligand field splitting of the molecular orbitals involved and thus in smaller *g*-values.

Furthermore, from a chemical point of view, CO would not bind to Ni^{3+}. The reason is that carbon monoxide is a weak σ donor and a strong π acceptor. Therefore, in a Ni^{3+} situation, CO would have to donate the lone pair to nickel, but the back donation from nickel to CO, which would stabilize the bond, is not feasible due to the large positive charge on the Ni^{3+}. Density functional theoretical studies are also consistent with a monovalent nickel center in both Ni–CO and Ni–L states [63], where the *g*-values and the ^{13}CO hyperfine parameters were in good agreement with the experimental data [32,63]. We thus conclude that the Ni in the Ni–CO and Ni–L states is formally monovalent Ni^{1+} and therefore the paramagnetic Ni–CO can be obtained only upon interaction of carbon monoxide with the light-induced Ni–L state.

5. Conclusions

The current study presents results on the characterization of the CO-inhibited states in the [NiFe] hydrogenase from *D. vulgaris* Miyazaki F by FTIR and EPR spectroscopies. A paramagnetic CO-inhibited state can be formed by treating a solution containing Ni–C with carbon monoxide followed by illumination to generate Ni–L, in which the nickel ion is in the 1+ state (monovalent). Based on the different rebinding kinetics during dark adaptation, binding of CO to Ni–L is favored as compared to the insertion of the hydride. The resulting Ni–CO state is proposed to be monovalent since it can be obtained only upon interaction of CO with Ni–L. On the other hand, two diamagnetic CO-bound complexes, Ni–SCO and Ni–SCO_{red}, can be formed by the binding of carbon monoxide to the active form Ni–SI_a. The one-electron difference between the latter is attributed to the reduction of the proximal [4Fe4S] cluster. At negative redox potentials below −500 mV, the Ni–CO bond can be "electrochemically cleaved" and the enzyme can recover its enzymatic activity despite the presence of CO in solution. Previous studies for enzymes derived from different organisms exhibited similar results. Differences are found for the absolute values of the redox potentials of the respective processes and for the extent of the CO "electrochemical detachment". Furthermore, in our experiments neither $(Ni–SI_r)_I$ nor Ni–C was shown to interact with CO. A rapid-scan FTIR study on the kinetics of the CO rebinding to the active site quantified for the first time the activation barrier for such a process, showing a weak metal carbonyl in the [NiFe] hydrogenases consistent with values reported for other metalloproteins such as myoglobin.

[5] Ni^{1+} spectra of model compounds are described by an axial *g*-tensor, but depending on the ligands they can also show a rhombic *g*-tensor. The distinction between Ni^{1+} and Ni^{3+} is not straightforward from EPR. Ni^{1+} would be in agreement with a d^9 configuration and the unpaired electron in the d_{x2-y2} orbital. However, the energy difference between the d_z^2 and d_{x2-y2} orbitals might not be large in this case, which would result in a significant mixing of these two orbitals [64].

Acknowledgment

Kim Bagley, Zhujun Chen and Shan Huang (Buffalo State University, NY) are gratefully acknowledged for sharing their previous observations on the light sensitivity related to the *D. vulgaris* and *A. vinosum* hydrogenases. Stimulating remarks and discussions with Helmut Görner (Max-Planck-Institut für Bioanorganische Chemie), Harry B. Gray (California Institute of Technology) and Thomas G. Spiro (Princeton University) are also gratefully acknowledged. The authors express their gratitude to Patricia Malkowski for the protein purification and to Gudrun Klihm, Frank Reikowski, Christoph Laurich, Rita Gröver and Birgit Deckers for technical support and assistance. This work was supported by the Max Planck Society, the EU/Energy Network Project SOLAR-H2 (FP7 Contract 212508) and BMBF (Bio H2, 03SF0355C).

Appendix A. Supplementary data

Supplementary data associated with this article can be found, in the online version, at doi:10.1016/j.bbabio.2009.11.002.

References

[1] P.M. Vignais, B. Billoud, Occurrence, classification, and biological function of hydrogenases: an overview, Chem. Rev. 107 (2007) 4206–4272.
[2] L.G. Ljungdahl, M.W. Adams, L.L. Barton, J.G. Ferry, M.K. Johnson, Biochemistry and Physiology of anaerobic Bacteria, Springer, New York, 2007.
[3] S.P.J. Albracht, Nickel hydrogenases: in search of the active site, Biochim. Biophys. Acta 1188 (1994) 167–204.
[4] W. Lubitz, E.J. Reijerse, M. van Gastel, [NiFe] and [FeFe] hydrogenases studied by advanced magnetic resonance techniques, Chem. Rev 107 (2007) 4331–4365.
[5] J.C. Fontecilla-Camps, A. Volbeda, C. Cavazza, Y. Nicolet, Structure/function relationships of [NiFe]- and [FeFe]-hydrogenases, Chem. Rev. 107 (2007) 4273–4303.
[6] Y. Nicolet, B.J. Lemon, J.C. Fontecilla-Camps, J.W. Peters, A novel FeS cluster in Fe-only hydrogenases, Trends Biochem. Sci. 25 (2000) 138–143.
[7] A. Silakov, E.J. Reijerse, S.P.J. Albracht, E.C. Hatchikian, W. Lubitz, The electronic structure of the H-cluster in the [FeFe]-hydrogenase from *Desulfovibrio desulfuricans*: a Q-band Fe-57-ENDOR and HYSCORE study, J. Am. Chem. Soc. 129 (2007) 11447–11458.
[8] S. Shima, O. Pilak, S. Vogt, M. Schick, M.S. Stagni, W. Meyer-Klaucke, E. Warkentin, R.K. Thauer, U. Ermler, The crystal structure of [Fe]-hydrogenase reveals the geometry of the active site, Science 321 (2008) 572–575.
[9] T. Yagi, K. Kimura, H. Daidoji, F. Sakai, S. Tamura, H. Inokuchi, Properties of purified hydrogenase from particulate fraction of *Desulfovibrio vulgaris* Miyazaki, J. Biochem. 79 (1976) 661–671.
[10] Y. Higuchi, T. Yagi, N. Yasuoka, Unusual ligand structure in Ni–Fe active center and an additional Mg site in hydrogenase revealed by high resolution X-ray structure analysis, Structure 5 (1997) 1671–1680.
[11] A. Volbeda, M.H. Charon, C. Piras, E.C. Hatchikian, M. Frey, J.C. Fontecilla-Camps, Crystal structure of the nickel–iron hydrogenase from *Desulfovibrio gigas*, Nature 373 (1995) 580–587.
[12] S.P.J. Albracht, Nickel Hydrogenases - in Search of the Active-Site. Biochim. Biophys. Acta 1188 (1994) 167–204.
[13] A.J. Pierik, W. Roseboom, R.P. Happe, K.A. Bagley, S.P.J. Albracht, Carbon monoxide and cyanide as intrinsic ligands to iron in the active site of [NiFe]-hydrogenases—NiFe(CN)(2)CO, biology's way to activate H-2, J. Biol. Chem. 274 (1999) 3331–3337.
[14] A. Volbeda, C. Piras, A.L. De Lacey, V.M. Fernandez, E.C. Hatchikian, M. Frey, J.C. Fontecilla-Camps, Structure of the [NiFe] hydrogenase active site: evidence for biologically uncommon Fe ligands, J. Am. Chem. Soc. 118 (1996) 12989–12996.
[15] Y. Higuchi, H. Ogata, K. Miki, N. Yasuoka, T. Yagi, Removal of the bridging ligand atom at the Ni–Fe active site of [NiFe] hydrogenase upon reduction with H-2, as revealed by X-ray structure analysis at 1.4 angstrom resolution, Structure 7 (1999) 549–556.
[16] J.M.C. Coremans, J.W. Van der Zwaan, S.P.J. Albracht, Distinct redox behavior of prosthetic groups in ready and unready hydrogenase from *Chromatium vinosum*, Biochim. Biophys. Acta 1119 (1992) 157–168.

[17] Y. Higuchi, S. Bando, M. Kusunoki, Y. Matsuura, N. Yasuoka, M. Kakudo, T. Yamanaka, T. Yagi, H. Inokuchi, The structure of cytochrome c_3 from *Desulfovibrio vulgaris* Miyazaki at 2.5-A resolution, J. Biochem. 89 (1981) 1659–1662.
[18] S. Dementin, B. Burlat, A.L. De Lacey, G. Adryanczyk-Perrier, B. Guigliarelli, V.M. Fernandez, M. Rousset, A glutamate is the essential proton transfer gate during the catalytic cycle of the [Ni–Fe] hydrogenase, J. Biol. Chem. 279 (2003) 10508–10513.
[19] M. van Gastel, C. Fichtner, F. Neese, W. Lubitz, EPR experiments to elucidate the structure of the ready and unready states of the [NiFe] hydrogenase of *Desulfolvibrio vulgaris* Miyazaki F,, Biochem. Soc. Trans. 33 (2005) 7–11.
[20] A.K. Jones, S.E. Lamle, H.R. Pershad, K.A. Vincent, S.P.J. Albracht, F.A. Armstrong, Enzyme electrokinetics: electrochemical studies of the anaerobic interconversions between active and inactive states of *Allochromatium vinosum* [NiFe]-hydrogenase, J. Am. Chem. Soc. 125 (2003) 8505–8514.
[21] S.E. Lamle, S.P.J Albracht, F.A. Armstrong, Electrochemical potential-step investigations of the aerobic interconversions of [NiFe]-hydrogenase from *Allochromatium vinosum*: insights into the puzzling difference between unready and ready oxidized inactive states, J. Am. Chem. Soc. 126 (2004) 14899–14909.
[22] V.M. Fernandez, E.C. Hatchikian, D.S. Patil, R. Cammack, ESR-detectable nickel and iron–sulfur centers in relation to the reversible activation of *Desulfovibrio gigas* hydrogenase, Biochim. Biophys. Acta 883 (1986) 145–154.
[23] A. Volbeda, L. Martin, C. Cavazza, M. Matho, B.W. Faber, W. Roseboom, S.P.J. Albracht, E. Garcin, M. Rousset, J.C. Fontecilla-Camps, Structural differences between the ready and unready oxidized states of [NiFe] hydrogenases, J. Biol. Inorg. Chem. 10 (2005) 239–249.
[24] H. Ogata, S. Hirota, A. Nakahara, H. Komori, N. Shibata, T. Kato, K. Kano, Y. Higuchi, Activation process of [NiFe] hydrogenase elucidated by high-resolution X-ray analyses: conversion of the ready to the unready state, Structure 13 (2005) 1635–1642.
[25] A.L. De Lacey, E.C. Hatchikian, A. Volbeda, M. Frey, J.C. Fontecilla-Camps, V.M. Fernandez, Infrared spectroelectrochemical characterization of the [NiFe] hydrogenase of *Desulfovibrio gigas*, J. Am. Chem. Soc. 119 (1997) 7181–7189.
[26] C. Fichtner, C. Laurich, E. Bothe, W. Lubitz, Spectroelectrochemical characterization of the [NiFe] hydrogenase of *Desulfovibrio vulgaris* Miyazaki F, Biochemistry 45 (2006) 9706–9716.
[27] B. Bleijlevens, F.A. van Broekhuizen, A.L. De Lacey, W. Roseboom, V.M. Fernandez, S.P.J. Albracht, The activation of the [NiFe]-hydrogenase from *Allochromatium vinosum*. An infrared spectro-electrochemical study, J. Biol. Inorg. Chem. 9 (2004) 743–752.
[28] M. Brecht, M. van Gastel, T. Buhrke, B. Friedrich, W. Lubitz, Direct detection of a hydrogen ligand in the [NiFe] center of the regulatory H-2-sensing hydrogenase from *Ralstonia eutropha* in its reduced state by HYSCORE and ENDOR spectroscopy, J. Am. Chem. Soc. 125 (2003) 13075–13083.
[29] S. Foerster, M. van Gastel, M. Brecht, W. Lubitz, An orientation-selected ENDOR and HYSCORE study of the Ni–C active state of *Desulfovibrio vulgaris* Miyazaki F hydrogenase, J. Biol. Inorg. Chem. 10 (2005) 51–62.
[30] P. Kellers, M.E. Pandelia, L.J. Currell, H. Görner, W. Lubitz, FTIR study on the light sensitivity of the [NiFe] hydrogenase from *Desulfovibrio vulgaris* Miyazaki F: Ni–C to Ni–L photoconversion, kinetics of proton rebinding and H/D isotope effect, Phys. Chem. Chem. Phys. 11 (2009) 8680–8683.
[31] A.L. De Lacey, V.M. Fernandez, M. Rousset, R. Cammack, Activation and inactivation of hydrogenase function and the catalytic cycle: spectroelectrochemical studies, Chem. Rev. 107 (2007) 4304–4330.
[32] J.W. van der Zwaan, S.P.J. Albracht, R.D. Fontijn, Y.B.M. Roelofs, EPR evidence for direct interaction of carbon monoxide with nickel in hydrogenase from *Chromatium vinosum*, Biochim. Biophys. Acta 872 (1986) 208–215.
[33] G.D. Fauque, Y.M. Berlier, E.S. Choi, H.D. Peck, J. LeGall, P.A. Lespinat, The carbon-monoxide inhibition of the proton deuterium-exchange activity of iron, nickel–iron and nickel–iron–selenium hydrogenases from *Desulfovibrio vulgaris* Hildenborough, Biochem. Soc. Trans. 15 (1987) 1050–1051.
[34] H. Ogata, Y. Mizoguchi, N. Mizuno, K. Miki, S. Adachi, N. Yasuoka, T. Yagi, O. Yamauchi, S. Hirota, Y. Higuchi, Structural studies of the carbon monoxide complex of [NiFe] hydrogenase from *Desulfovibrio vulgaris* Miyazaki F: suggestion for the initial activation site for dihydrogen, J. Am. Chem. Soc. 124 (2002) 11628–11635.
[35] R.P. Happe, W. Roseboom, S.P.J. Albracht, Pre-steady-state kinetics of the reactions of [NiFe]-hydrogenase from *Chromatium vinosum* with H_2 and CO, Eur. J. Biochem. 259 (1999) 602–608.
[36] A.L. De Lacey, C. Stadler, V.M. Fernandez, E.C. Hatchikian, H.J. Fan, S.H. Li, M.B. Hall, IR spectroelectrochemical study of the binding of carbon monoxide to the active site of *Desulfovibrio fructosovorans* Ni–Fe hydrogenase, J. Biol. Inorg. Chem. 7 (2002) 318–326.
[37] K.A. Bagley, C.J. van Garderen, M. Chen, E.C. Duin, S.P.J. Albracht, W.H. Woodruff, Infrared studies on the interaction of carbon monoxide with divalent nickel in hydrogenase from *Chromatium vinosum*, Biochemistry 33 (1994) 9229–9236.
[38] S.J. George, S. Kurkin, R.N.F. Thorneley, S.P.J. Albracht, Reactions of H-2, CO, and O-2 with active [NiFe]-hydrogenase from *Allochromatium vinosum*. A stopped-flow infrared study, Biochemistry 43 (2004) 6808–6819.
[39] D.A. Moss, M. Leonhard, M. Bauscher, W. Mantele, Electrochemical redox titration of cofactors in the reaction center from *Rhodobacter sphaeroides*, FEBS Lett. 283 (1991) 33–36.
[40] F. Baymann, D.A. Moss, W. Mantele, An electrochemical assay for the characterization of redox proteins from biological electron-transfer chains, Anal. Biochem. 199 (1991) 269–274.
[41] M.L. Fultz, R.A. Durst, Mediator compounds for the electrochemical study of biological redox systems—a compilation, Anal. Chim. Acta 140 (1982) 1–18.
[42] P. Atkins, J. Paula, Atkins' physical chemistry, Oxford Univ. Press, 2006.
[43] M.Y. Darensbourg, E.J. Lyon, J.J. Smee, The bio-organometallic chemistry of active site iron in hydrogenases, Coord. Chem. Rev. 206 (2000) 533–561.
[44] M.E. Pandelia, H. Ogata, L.J. Currell, M. Flores, W. Lubitz, Probing intermediates in the activation cycle of [NiFe] hydrogenase by infrared spectroscopy: the Ni–SIr state and its light sensitivity, J. Biol. Inorg. Chem. 14 (2009) 1227–1241.
[45] R.A. Nyquist, The significance of temperature and solvent effects upon infrared spectra and group frequencies, Appl. Spectrosc. 40 (1986) 79–85.
[46] O. Sorgenfrei, A. Klein, S.P.J. Albracht, Influence of illumination on the electronic interaction between Se-77 and nickel in active F420-non-reducing hydrogenase from *Methanococcus voltae*, FEBS Lett. 332 (1993) 291–297.
[47] J.P. Collman, J.I. Brauman, K.M. Doxsee, Carbon-monoxide binding to iron porphyrins, Proc. Natl. Acad. Sci. U. S. A. 76 (1979) 6035–6039.
[48] C. Leger, S. Dementin, P. Bertrand, M. Rousset, B Guigliarelli, Inhibition and anaerobic inactivation kinetics of *Desulfovibrio fructosovorans* NiFe hydrogenase studied by protein film voltammetry, J. Am. Chem. Soc. 126 (2004) 12162–12172.
[49] S. Kurkin, S.J. George, R.N.F Thorneley, S.P.J. Albracht, Hydrogen-induced activation of the [NiFe]-hydrogenase from *Allochromatium vinosum* as studied by stopped-flow infrared spectroscopy, Biochemistry 43 (2004) 6820–6831.
[50] M. Bruschi, L. De Gioia, G. Zampella, M. Reiher, P. Fantucci, M. Stein, A theoretical study of spin states in Ni–S_4 complexes and models of the [NiFe] hydrogenase active site, J. Biol. Inorg. Chem. 9 (2004) 873–884.
[51] A. Pardo, A.L. De Lacey, V.M. Fernandez, H.J. Fan, Y. Fan, M.B. Hall, Density functional study of the catalytic cycle of nickel-iron [NiFe] hydrogenases and the involvement of high-spin nickel (II) J, Biolog. Inorg. Chem. 11 (2006) 286–306.
[52] Y.M. Berlier, G.D. Fauque, J. LeGall, P.A. Lespinat, H.D. Peck, The activation of the periplasmic (NiFe) hydrogenase of *Desulfovibrio gigas* by carbon monoxide, FEBS Lett. 221 (1987) 241–244.
[53] S.E. Lamle, S.P.J. Albracht, F.A. Armstrong, The mechanism of activation of a [NiFe]-hydrogenase by electrons, hydrogen, and carbon monoxide, J. Am. Chem. Soc. 127 (2005) 6595–6604.
[54] C.H. Lai, W.Z. Lee, M.L. Miller, J.H. Reibenspies, D.J. Darensbourg, M.Y. Darensbourg, Responses of the Fe(CN)(2)(CO) unit to electronic changes as related to its role in [NiFe]hydrogenase, J. Am. Chem. Soc. 120 (1998) 10103–10114.
[55] M. Asso, B. Guigliarelli, T. Yagi, P. Bertrand, EPR and redox properties of *Desulfovibrio vulgaris* Miyazaki hydrogenase—comparison with the Ni–Fe enzyme from *Desulfovibrio gigas*, Biochim. Biophys. Acta 1122 (1992) 50–56.
[56] P.S. Braterman, Metal Carbonyl Spectra, Academic Press, London, 1975.
[57] F.A. Cotton, Vibrational spectra and bonding in metal carbonyls. III. Force constants and assignments of CO stretching modes in various molecules; evaluation of CO bond orders, Inorg. Chem. 3 (1964) 702–711.
[58] C.S. Kraihanzel, F.A. Cotton, Vibrational spectra and bonding in metal carbonyls. II. Infrared spectra of amine-substituted group VI carbonyls in the CO stretching region, Inorg. Chem. 2 (1963) 533–540.
[59] C. Fichtner, M. van Gastel, W. Lubitz, Wavelength dependence of the photo-induced conversion of the Ni–C to the Ni–L redox state in the [NiFe] hydrogenase of *Desulfovibrio vulgaris* Miyazaki F, Phys. Chem. Chem. Phys. 5 (2003) 5507–5513.
[60] H. Frauenfelder, S.G. Sligar, P.G. Wolynes, The energy landscapes and motions of proteins, Science 254 (1991) 1598–1603.
[61] F. Parak, H. Frauenfelder, Protein dynamics, Physica A 201 (1993) 332–345.
[62] R.H. Austin, K.W. Beeson, L. Eisenstein, H. Frauenfelder, I.C. Gunsalus, Dynamics of ligand binding to myoglobin, Biol. Phys. (1993).
[63] M. Stein, E. van Lenthe, E.J. Baerends, W. Lubitz, Relativistic DFT Calculations of the paramagnetic intermediates of [NiFe] hydrogenase. Implications for the enzymatic mechanism, J. Am. Chem. Soc. 123 (2001) 5839–5840.
[64] M. van Gastel, W. Lubitz, in: G.R. Hanson, L.J. Berliner (Eds.), High Resolution EPR: Applications to Metalloenzymes and Metals in Medicine, Biol. Magn. Res., vol. 28, Springer, New York, 2009, pp. 441–470.